Journal of Materials Chemistry A

Suppressing Pre-Aggregation to Increase Polymer Solar Cell Ink Shelf Life

Journal:	*Journal of Materials Chemistry A*
Manuscript ID	TA-COM-10-2023-006617
Article Type:	Communication
Date Submitted by the Author:	30-Oct-2023
Complete List of Authors:	Wang, Zhen; North Carolina State University, Physics Peng, Zhengxing; North Carolina State University, Balar, Nrup; North Carolina State University, Physics Ade, Harald; North Carolina State University, Physics

COMMUNICATION

Suppressing Pre-Aggregation to Increase Polymer Solar Cell Ink Shelf Life

Received 00th January 20xx,
Accepted 00th January 20xx

DOI: 10.1039/x0xx00000x

Zhen Wang, Zhengxing Peng, Nrup Balar, and Harald Ade*

Chemical degradation and morphology failure of ink-processed organic solar cells are now extensively studied. In contrast, the general problem that inks prepared via thermal and mechanical agitation degrade and age rapidly at room temperature has yet to be delineated as a commercialization bottleneck and resolved. This study unveils the intrinsic aging of common polymer:nonfullerene acceptor (NFA) binary inks and the impact of electro-optically active component additives on ink shelf life. As a result, we developed an effective approach to slow down the ink aging by employing an additive (i.e. PCBM variants) with high miscibility with the polymer and NFA. It is inferred that the PCBM in the inks act as a co-solvent and slow down the polymer and possibly the NFA pre-aggregation, preventing the formation of large domains in the films. At the same time, the PCBMs dissolved in the polymer-rich phase of the devices can maintain the electron percolations and hence benefit charge creation and collection. The method of introducing a hyper-miscible third component, that is with concentration above the percolation threshold, to improve ink shelf life as well as maintain the percolation is delineated for the first time. It represents a synergistic approach to promote the scale-up of ink-processed organic solar cells.

Organic solar cells (OSCs) with ink-processed photoactive layers have recently achieved power conversion efficiencies (PCEs) of over 18-19% in laboratories, after decades of efforts to design new materials and optimize device engineering and processing.[1-3] Further optimization of molecular modifications and ternary blending strategy is still intensively ongoing and pushing the efficiencies towards the Shockley–Queisser limit.[4-6] Reports of large-area modules on rigid and flexible substrates are making it possible to be industrially manufactured, owing to their excellent ability to be ink-processed.[7-11] However, critical challenges of stability still remain to be overcome for their commercialization.[12-14] Without decent stability and long enough lifetime with consistent performance, OSC products are still too immature to be utilized in and applied to our real life.

The instabilities of OSCs stem from a number of factors, such as oxygen and/or moisture sensitivity,[15] surface-assisted photoreaction,[16, 17] electrode/interlayer degradation[18, 19] and morphology failure.[20, 21] With proper device engineering and encapsulation, issues from the outside and interfaces can be significantly suppressed. We have previously been focusing on the morphology stability, which is one of the intrinsic instabilities that needs to be understood and controlled. Ghasemi et al. have developed the Ade-O'Connor-Ghasemi interaction–diffusion framework for predicting OSC stability of binaries and revealed that the thermodynamically most unstable, hypo-miscible systems are the most kinetically stabilized.[22, 23] That said, the use of a ternary component with high miscibility to maintain charge percolation (a system referred as hyper-miscible) and high glass transition temperature (for a given molecule size) to slow down the diffusion in order to achieve an ultra-stable morphology is conceptually desirable but faces practical hurdles as these demands are not favored thermodynamically.[24, 25]

All the above studies have concentrated on the stability of practical OSC devices, while studies are rarely reported about the pre-fabrication requirements for commercialization and their underlying molecular interactions. Generally, when fabricating the devices, freshly dissolved solutions/inks are made and used to spin-cast the photoactive layers. In our experiences, OSCs made with aged inks usually exhibit poorer performance than that made from fresh inks, and some aged inks are even unable to be restored and reused after only a few hours.[26] It is already reported that the molecules in the inks can pre-aggregate as solutions cool for materials that show strong temperature dependent aggregation, which plays a critical role in the film molecular packing and morphology as solvent evaporates during processing and the concentration increases. Such aggregation depends on the molecular self-interaction and the interaction with the solvent.[27] In principle, any ink made by heating the solution is likely subjected to pre-aggregation that limits ink shelf life. For future fabrication and manufacture and even for now in laboratories, this current necessity of using fresh inks is leading to significant waste of photovoltaic materials or contributes to reproducibility issues and narrow fabrication windows. Due to reduced solubility, aging is particularly rapid from non-chlorinated solvents such as o-xylene explored to upscale printing with an acceptable environmental footprint. So, understanding the reason of ink degradation and aging and finding a way to slow it down or

Department of Physics and Organic and Carbon Electronics Laboratories (ORaCEL), North Carolina State University, Raleigh, NC 27695, United States.
**Email: hwade@ncsu.edu*
†Electronic Supplementary Information (ESI) available: Experimental Section, Figs. S1–S15, and Table S1-S6. See DOI: 10.1039/x0xx00000x

prevent it altogether is very important to reducing engineering bottlenecks to industrial production. In industrial production, material synthesis, ink preparation, device fabrication, and encapsulation etc. may be done by different production lines, and are not necessarily done within one day. Ideally, inks are like premixed paints and can be purchased and used as needed. We target to achieve this convenience by improving ink stability, as ink aging and ink consumption is considered one of the hindrances to the commercialization of OSCs.

In this manuscript, we report thermodynamic properties of active materials as they relate to ink aging. We start by unveiling the ink aging of D18-Cl:Y6 blend[28] and demonstrate an effective approach to suppress the observed significant ink aging by employing third components ($PC_{61}BM$ or $PC_{71}BM$) that we show to have high miscibility with the polymer and Y6. Molecular structures of these compounds can be found in **Fig. 1a**. The D18-Cl:Y6 binary system shows a decreasing fill factor (FF) as the ink ages. Devices made from fresh ink exhibit an FF of 75.2%, and those made from 5-day- and 20-day-aged inks show poor FFs of 70.5% and 61.1%, respectively. With the PCBMs as third components, the ternary devices made from (20-day) aged inks still show decent FFs of over 70%. We have employed molecular packing, morphology and thermodynamic characterizations to figure out the reason. X-ray scattering experiments reveal that the molecular packing of binary and ternary films cast from fresh and aged inks are very similar. In contrast, the long period (related to domain size) of the films is found to be larger when cast from aged inks for the binary blend while not for the ternary blends. The miscibility of D18-Cl:Y6 is determined to be small (few %) at room temperature. In contrast, the PCBMs exhibit quite large miscibilities (>50%) with the D18-Cl and Y6. In contrast, perylene red has low miscibility with D18-Cl and cannot suppress the ink aging. We have attributed the deceleration of ink aging to PCBMs suppressing the pre-aggregation of the polymer and likely Y6 in inks. This suppression of ink aging by introducing a highly miscible acceptor also works for the PM6:Y6 system, as observed during an initial assessment of the generality of our findings. An added synergistic benefit is that the high miscibility of the fullerenes maintains percolation pathways for electrons and also stabilizes devices. Our approach of introducing a highly miscible third component to suppress the ink aging as well as maintain the percolation is of significant importance to promote the scale-up of low-cost ink-processed polymer solar cells and hence a step to their commercialization.

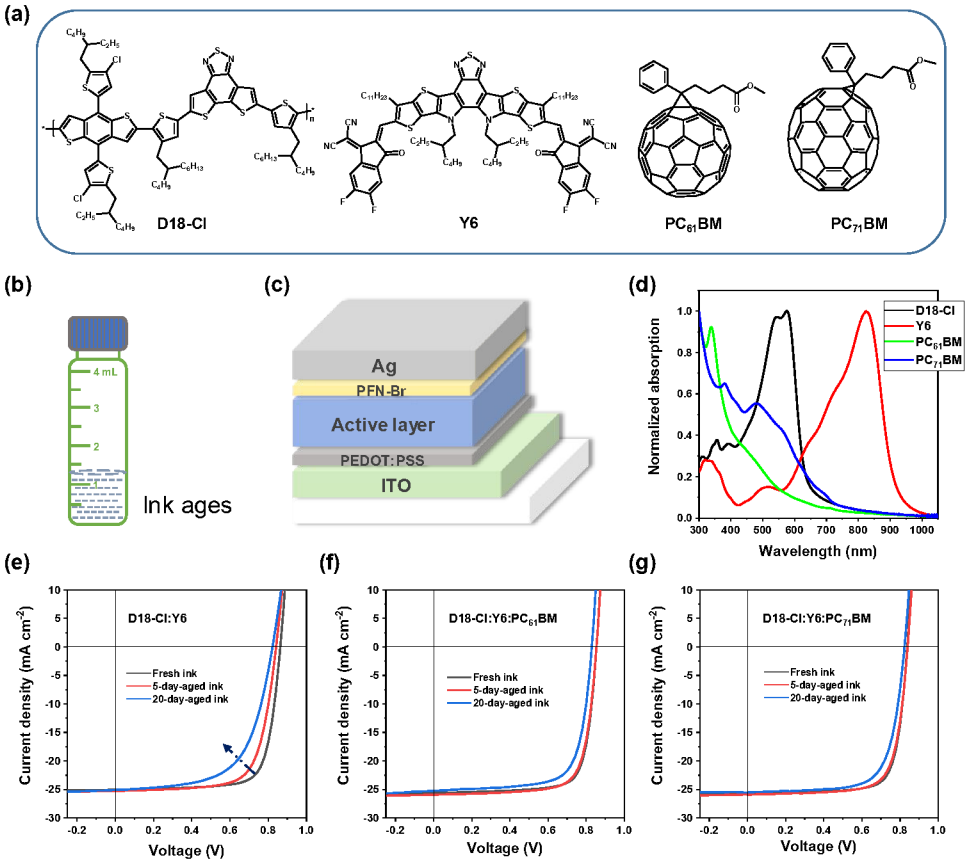

Fig. 1. (a) Molecular structures of D18-Cl, Y6, $PC_{61}BM$ and $PC_{71}BM$. (b) An illustration of ink aging in glass vials. (c) An illustration of the regular device architecture used in this work. (d) UV-vis absorption spectra of D18-Cl, Y6, $PC_{61}BM$ and $PC_{71}BM$ films. (e–g) J–V curves of devices based on D18-Cl:Y6 (e), D18-Cl:Y6:$PC_{61}BM$ (f) and D18-Cl:Y6:$PC_{71}BM$ (g) blends, with photoactive layers cast from fresh, 5-day-aged, and 20-day-aged inks.

We explored ink-aging based-on the high efficiency D18-Cl:Y6 binary and ternary blends with two PCBMs ($PC_{61}BM$ and $PC_{71}BM$). The illustrations of inks used and the device architecture are shown in **Fig. 1b** and **c**, respectively. Details of fabrication recipe can be found in the Experimental Section in Supplementary Information. **Fig. 1d** shows the normalized ultraviolet-visible (UV-vis) absorption of D18-Cl, Y6 and PCBM films. The binary solar cells based on D18-Cl:Y6 from fresh inks exhibit an average PCE of 16.18% with an open-circuit voltage (V_{OC}) of 0.849, a short-circuit current density (J_{SC}) of 25.33 mA cm^{-2}, and an FF of 75.2%. While after 5 days, the very same batch of ink gives a PCE of 15.01% with a V_{OC} of 0.84 and a decreased FF of 70.5%. Aged for 20 days, devices fabricated from the ink perform a PCE of 12.37% (which is only 76% of that made from fresh ink), with a lower V_{OC} of 0.82 and a poor FF of 61.1%. Clearly the binary ink can age quite pronounced within only a few days, even when the vial is sealed properly and stored in the dark and in a nitrogen atmosphere.

Knowing that PCBMs can be highly miscible with some donor polymer that improves the performance and stability of many other binary nonfullerene systems, in large part by maintaining percolation (electron pathways) and hence suppress the degradation that comes from over-purification of mixed disorder domains,[24] we employed PCBM as third components to investigate the ink aging and relations to miscibility. The ternary solar cells based on D18-Cl:Y6:$PC_{61}BM$ from fresh inks exhibit a slightly improved PCE of 16.54%, with a V_{OC} of 0.849, a J_{SC} of 25.43 mA cm^{-2}, and an FF of 76.6%. Importantly, the ternary solar cells fabricated from 5-day-aged ink still give a PCE of 16.15%, with a V_{OC} of 0.845, a J_{SC} of 25.53 mA cm^{-2}, and an FF of 74.8%. Even the devices made from 20-day-aged ink perform with an efficiency of 15.02%, with a V_{OC} of 0.831, a J_{SC} of 25.20 mA cm^{-2}, and an FF of 71.7%. In the case of $PC_{71}BM$, the trend is quite similar. The current density–voltage (*J*–*V*) curves corresponding to the binary and ternary devices are shown in **Fig. 1e**-**g**, and the photovoltaic parameters are summarized in **Table 1**. It seems that though the ternary inks with PCBMs also age, but this aging is significantly reduced compared to the binary one. After 20 days, the aged ternary inks can still give FFs of over 70%, while the binary one already decreased to ~60%. **Fig. S1** shows the normalized UV-vis absorption spectra of D18-Cl:Y6, D18-Cl:Y6:$PC_{61}BM$, and D18-Cl:Y6:$PC_{71}BM$ blend films, cast from fresh, 5-day-aged and 20-day-aged inks, respectively. No pronounced differences can be distinguished from the fresh inks and 5-day-aged inks, which is likely because that the aging has limited impact to the molecular packing and optical, local aggregation effects. But after 20-days aging, the absorption intensities corresponding to D18-Cl become relatively smaller in all three systems.

To understand the differences of devices made from fresh and aged inks, we have conducted grazing incidence wide angle X-ray scattering (GIWAXS) and resonant soft X-ray scattering (R-SoXS) to probe the molecular packing and in-plane morphology of the photoactive layers. **Fig. S2** shows the 2D GIWAXS patterns of neat D18-Cl and Y6 films. The D18-Cl also shows the (00*l*) diffraction peaks as D18 exhibits strong chain extension.[26] And **Figs. S3**-**S5** displays the 2D GIWAXS patterns of binary and ternary blend films based on D18-Cl:Y6, D18-Cl:Y6:$PC_{61}BM$ and D18-Cl:Y6:$PC_{71}BM$, respectively, cast from fresh, 5-day- and 20-day-aged inks. The corresponding 1D profiles along out-of-plane (OOP) and in-plane (IP) directions are shown in **Fig. 2a**-**b**. The related information of coherence lengths (L_C) and *g* parameters are calculated and summarized in **Table S1**.[29] The GIWAXS data analysis shows that the molecular packing and quality of ordering are not changing much relative to fresh inks when films are cast from aged inks, which is consistent with the UV-vis absorption spectra.

Table 1. Summary of photovoltaic performance of devices fabricated from fresh and aged inks.

Blends	V_{OC} (V)	J_{SC} (mA cm^{-2})	FF (%)	PCE_{avg} (%)	PCE_{max} (%)
D18-Cl:Y6 fresh ink	0.849 ± 0.009	25.33 ± 0.17	75.2 ± 0.5	16.18 ± 0.20	16.62
D18-Cl:Y6 5-day-aged ink	0.840 ± 0.003	25.32 ± 0.21	70.5 ± 0.6	15.01 ± 0.18	15.25
D18-Cl:Y6 20-day-aged ink	0.820 ± 0.010	24.66 ± 0.35	61.1 ± 1.2	12.37 ± 0.44	12.87
D18-Cl:Y6:$PC_{61}BM$ fresh ink	0.849 ± 0.005	25.43 ± 0.32	76.6 ± 0.8	16.54 ± 0.36	17.15
D18-Cl:Y6:$PC_{61}BM$ 5-day-aged ink	0.845 ± 0.005	25.53 ± 0.30	74.8 ± 0.3	16.15 ± 0.23	16.56
D18-Cl:Y6:$PC_{61}BM$ 20-day-aged ink	0.831 ± 0.007	25.20 ± 0.20	71.7 ± 0.6	15.02 ± 0.20	15.21
D18-Cl:Y6:$PC_{71}BM$ fresh ink	0.836 ± 0.003	25.31 ± 0.46	77.2 ± 0.3	16.33 ± 0.31	16.76
D18-Cl:Y6:$PC_{71}BM$ 5-day-aged ink	0.845 ± 0.009	25.68 ± 0.18	74.7 ± 0.1	16.23 ± 0.30	16.62
D18-Cl:Y6:$PC_{71}BM$ 20-day-aged ink	0.826 ± 0.003	25.09 ± 0.30	70.9 ± 0.6	14.70 ± 0.24	14.98

Device performance was averaged from 12 cells.

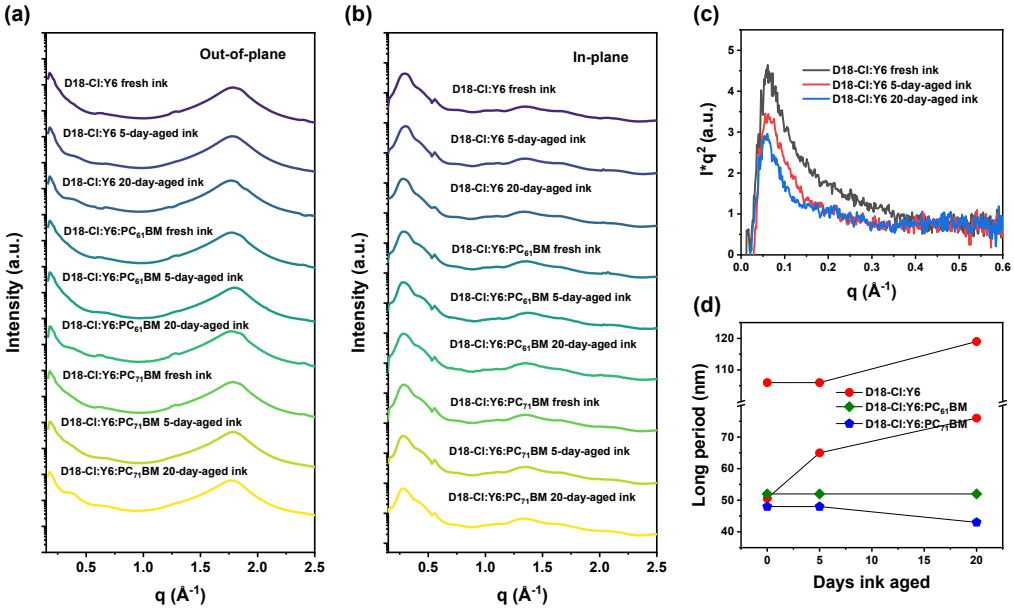

Fig. 2. (a-b) 1D GIWAXS profiles of films based on D18-Cl:Y6, D18-Cl:Y6:$PC_{61}BM$ and D18-Cl:Y6:$PC_{71}BM$ blends, cast from fresh, 5-day-aged, and 20-day-aged inks, along OOP (a) and IP (b) directions. (c) Lorentz-corrected thickness-normalized R-SoXS profiles of films based on D18-Cl:Y6 cast from fresh, 5-day-aged, and 20-day-aged inks, acquired at 283.8 eV. (d) Long period obtained from R-SoXS profiles of D18-Cl:Y6, D18-Cl:Y6:$PC_{61}BM$ and D18-Cl:Y6:$PC_{71}BM$ blends as a function of ink aging days.

The R-SoXS profiles of the D18-Cl systems show strong fluorescence backgrounds, especially with X-ray energies above the C-1s absorption onset. We correct this unfavorable background[30] and extract the long period information from the diffraction features of R-SoXS profiles acquired at low energies. The Lorentz-corrected and thickness-normalized R-SoXS profiles of films based on D18-Cl:Y6, D18-Cl:Y6:$PC_{61}BM$ and D18-Cl:Y6:$PC_{71}BM$ blends, cast from fresh, 5-day- and 20-day-aged inks, acquired at 283.8 eV, are displayed respectively in **Fig. 2c**, **Fig. S6a** and **b**. As can be seen in **Fig. 2**c, the peak positions of D18-Cl:Y6 blend films show a clearly decreasing trend as the ink ages, which corresponds to an increasing long period and thus larger domain size.[31] We employed lognormal functions to fit the peaks and obtained the peak positions (see **Fig. S7)**. The binary system can be fit roughly with two lognormal peaks, indicating a hierarchical or multi-length scale morphology. For the film cast from fresh ink, two peaks are located at q = 0.059 and 0.124 nm^{-1}, corresponding to long periods of 106 and 50.6 nm, respectively. For devices cast from 5-day-aged ink, the two peaks are located at q = 0.059 and 0.096 nm^{-1}, corresponding to long periods of 106 and 65 nm, respectively. While for the film cast from 20-day-aged ink, the two peaks moved to q = 0.053 and 0.082 nm^{-1}, corresponding to long periods of 119 and 76 nm, respectively. The trends in domain size observed with R-SoXS should be attributed to the unfavorable molecular pre-aggregation of the inks as they age at room temperature.[27]

In contrast to the binaries, the R-SoXS profiles of the ternary blend films with $PC_{61}BM$ from fresh and aged inks (**Fig. S6a**) are quite similar to each other and only one lognormal peak can be distinguished. The fitting is displayed in **Fig. S8** and the peak positions are all estimated to be around 0.12 nm^{-1}, corresponding to long periods of 52 nm. The R-SoXS profiles of the ternary blend films with $PC_{71}BM$ from fresh and aged inks are shown in **Fig. S6b** and the fitting is shown in **Fig. S9**. For the ternary films cast from both fresh and 5-day-aged inks, one peak is fit and located at q = 0.130 nm^{-1}, corresponding to a long period of 48 nm. And for the film cast from 20-day-aged ink, one lognormal peak can be fit to be q = 0.146 nm^{-1}, corresponding to long periods of 43 nm. Similar to $PC_{61}BM$, the ternary blends with $PC_{71}BM$ can also benefit to small domains and suppress the polymer pre-aggregation during aging. A comparison of long periods is summarized in **Fig. 2d**. This indicates that the ternary blend with PCBM not only exhibits small domain sizes, which is favorable for charge generation, but also ink aging does not result in larger aggregates as a function of time as observed for the binary blend.

Though the R-SoXS results give us pretty clear mechanistic explanations of why the PCBMs could decelerate the ink aging, we delineate the thermodynamic nature of the binary and ternary systems to understand the molecular interactions that drive the observed improvements. To get more insights regarding the thermodynamic properties, time-of-flight secondary ion mass spectrometry (TOF-SIMS) was employed following prior established protocols to obtain the miscibility information between the donor and acceptor materials.[22, 32] **Fig. 3a** shows the TOF-SIMS profiles of D18-Cl/Y6 bilayer samples annealed at different temperatures, tracking F^- ion of the acceptor. And the corresponding miscibility information (Y6 fraction Φ_{Y6} as a function of temperature) of D18-Cl/Y6 is shown

in **Fig. 3b** along with a simulated binodal curve from the Flory–Huggins (FH) free energy of mixing equation for polymer inks with the actual molecular weights of the same system.[33] As can be seen from the upper critical solution temperature (UCST) phase diagram, the polymer D18-Cl and Y6 are hypo-miscible at low temperature (< 150 °C), that is, the binodal composition is smaller than the percolation threshold, and the critical temperature is around 250 °C. Using the FH fit, the miscibility of D18-Cl:Y6 at room temperature (RT) is estimated by extrapolation to be Φ_{Y6} = 2.6%. This value is similar to the ~3% derived by measurements on bilayers that were solvent vapor annealed (SVA) at RT with chlorobenzene (CB) (see **Fig. S10a**). This concentration is significantly below the percolation threshold that would maintain electron pathways and benefit the device performance.[34] Even when devices are quenched to mixed domain composition that is near the percolation of Φ_{NFA} = 20% – 30% when spin-casting from chloroform inks, this hypo-miscible nature of D18-Cl/Y6 is likely to lead to over-purification of the morphology during aging of the devices and hence degrade the devices. At the same time, the strong repulsive interactions between D18-Cl and Y6 makes Y6 a poor co-solvent in the ink.

To assess qualitatively the relative co-solvent effect of fullerenes, we also measured the molecular interdiffusion for D18-Cl/$PC_{61}BM$ and D18-Cl/$PC_{71}BM$ bilayers that have been SVA with CB at RT to promote molecular diffusion. The corresponding mass-normalized profiles of D18-Cl/$PC_{61}BM$ and D18-Cl/$PC_{71}BM$ bilayers, tracking S^- ion of the polymer, are shown in **Fig. 3c** and **d** respectively. It is readily visible that the polymer layer swells due to the significant incorporation of the PCBM with a corresponding miscibility of D18-Cl/ $PC_{61}BM$ is Φ_{PC61BM} ~ 60% and the miscibility of D18-Cl/$PC_{71}BM$ is Φ_{PC71BM} ~ 52% derived using prior protocols.[32] Both the PCBM variants show hyper-miscibility with the polymer D18-Cl. We note that the extensive swelling might have been restraint by tie-chains between paracrystallites, which would result in the measurements yielding a lower limit for the miscibility and the actually miscibility being even higher.[35] We also attempted to utilize our previously developed UV-vis absorption method to verify the miscibility derived from the TOF-SIMS results (see **Fig. S11**).[36] Unfortunately, the density of PCBMs domains/crystals formed by SVA did not allow analysis. This lack of strong phase separation and lack of PCBM crystal formation contrasts to the observation in immiscible systems and confirms the high miscibility of D18-Cl:PCBMs that we observe quantitatively with TOF-SIMS. Such high miscibility will maintain percolation and facilitate the flow of electrons from the acceptor phases through the mixed amorphous domains, consistent with prior works.[24, 25] Importantly, the high miscibility of the PCBM with D18-Cl likely makes PCBM an effective co-solvent that suppresses the polymer aggregation in the solution.

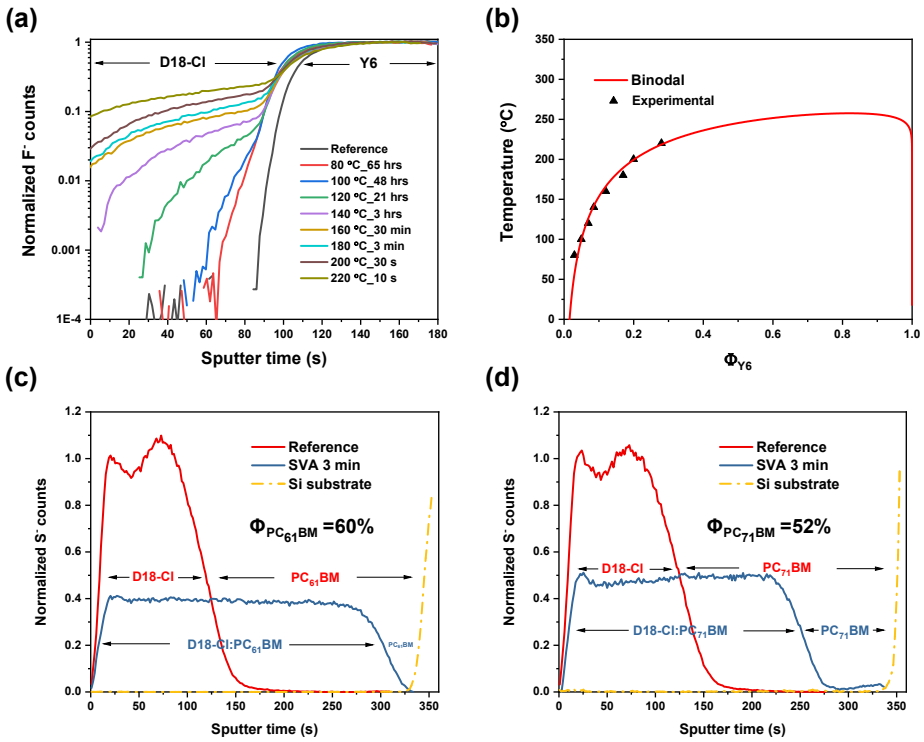

Fig. 3. (a) TOF-SIMS profiles of D18-Cl/Y6 bilayer samples annealed at different temperatures, tracking F^- ion of the acceptor. (b) Simulated binodal curve of D18-Cl/Y6 system along with the miscibility information (Y6 fraction Φ vs. temperature) measured with TOF-SIMS. (c-d) TOF-SIMS profiles of D18-Cl/$PC_{61}BM$ (c) and D18-Cl/$PC_{71}BM$ (d) bilayers solvent vapor annealed, tracking S^- ion of the polymer.

Due to the technical difficulty of floating small-molecule films on water, TOF-SIMS cannot be used to determine the Y6:PCBM miscibility. The UV-vis absorption method is then applied in this case, even though it does not yield the binodal but the liquidus composition. Due to added chemical potential of the crystals, only a lower limit of the miscibility can be derived. **Fig. 4** shows visible light microscopy (VLM) images of Y6:$PC_{61}BM$, and Y6:$PC_{71}BM$ blend films, SVA with CB for 48 h at RT, and the corresponding UV-vis absorption spectra. By fitting the absorption spectra of annealed blend films with the mass-thickness corrected absorption spectra of the neat films, we can estimate the lower limit of the miscibility of Y6:$PC_{61}BM$ to be $\Phi_{Y6} \approx 64\%$ and the miscibility of Y6:$PC_{71}BM$ to be $\Phi_{Y6} \approx 42\%$. When SVA at low temperature e.g. –2 °C, the miscibility of Y6:$PC_{61}BM$ is estimated to be $\Phi_{Y6} \approx 42\%$ and the miscibility of Y6:$PC_{71}BM$ is $\Phi_{Y6} \approx 28\%$ (shown in **Fig. S12**). The differences observed are consistent with an UCST phase diagram and indicate that the method measures meaningful relations. Furthermore, such high concentration of Y6 for the liquidus indicates that the critical temperature of the binodal is likely below room temperature and disordered Y6:PCBM are in the one-phase region at room temperature and intimately mixed.

To demonstrate that the PCBM suppresses ink aging and which factor is likely dominant, we have prepared and aged the donor (D18-Cl or D18-Cl:$PC_{61}BM$) and acceptor (Y6) solutions separately. D18-Cl:Y6 binary and (D18-Cl:$PC_{61}BM$):Y6 ternary inks were mixed together only immediately before device processing. A summary of device performance of D18-Cl:Y6 and (D18-Cl:$PC_{61}BM$):Y6 systems are tabulated in **Table S2**. The addition of PCBM is found again to significantly suppress the ink aging, with ternary devices experiencing a smaller loss in performance compared to the binary devices. Additionally, while preparing the inks, it was observed that the $PC_{61}BM$ can effectively reduce the stickiness/viscosity of D18-Cl in chloroform. This could be direct evidence that the PCBMs can suppress the pre-aggregation of the polymer even right after it is dissolved. Based on these characterizations, we have attributed ink stabilization by PCBM to the suppression the aggregation of the polymer in inks. A schematic of the PCBM suppressing the polymer aggregation in the inks is shown in **Fig. S13**.

In order to establish a control experiment, the small molecule perylene red (molecular structure is shown in **Fig. S14**) is introduced to D18-Cl:Y6 system to modulate the molecular interactions between additive and binary components. TOF-SIMS characterization results of D18-Cl/perylene red bilayers are shown in **Fig. S10b** along with the profiles of D18-Cl/Y6, and D18-Cl/PCBM bilayers for a clear comparison of the miscibilities. Perylene red shows a miscibility of around 10% with D18-Cl at room temperature, whereas the fullerenes had miscibilities larger than 50%. Photovoltaic performance of D18-Cl:Y6:perylene red devices fabricated from fresh and aged inks is summarized in **Table S3**. As a third component, perylene red could not reduce ink degradation during storage. The emerging proposed explanation is that small molecules that are highly miscible (>50%) with the polymer, i.e. PCBMs, can suppress the pre-aggregation and hence ink aging, while the additives, e.g. perylene red with small miscibility with the polymer can not. A similar argument will likely hold regarding a co-solvent effect for Y6.

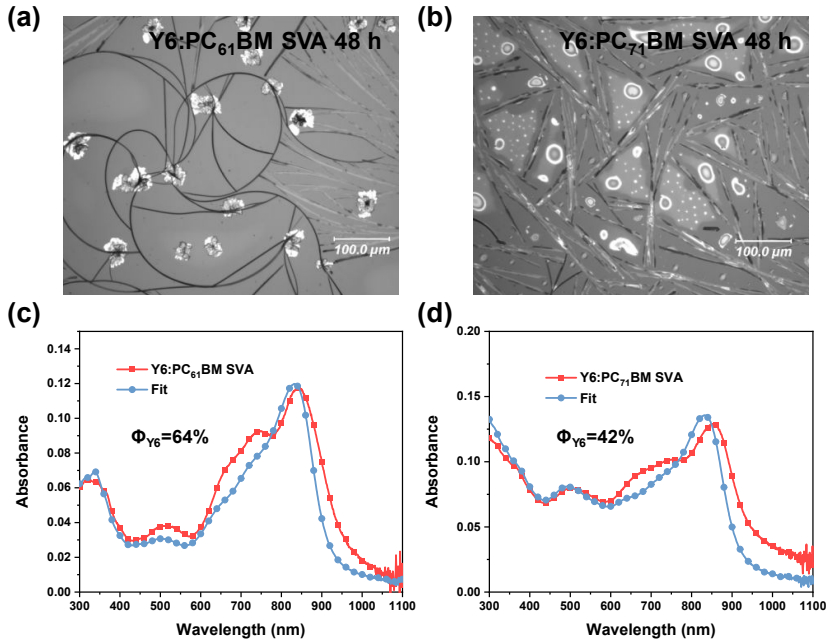

Fig. 4. (a-b) VLM images of Y6:$PC_{61}BM$, and Y6:$PC_{71}BM$ blend films, SVA with chlorobenzene for 48 h at room temperature. (c-d) UV-vis absorption spectra and fits of Y6:$PC_{61}BM$, and Y6:$PC_{71}BM$ blend films, SVA with chlorobenzene for 48 h at room temperature.

In a rudimentary confirmation of the co-solvent model, we turned to the PM6:Y6 system[37] as PCBM has been previously shown to be highly miscible with PM6.[34] Indeed, we found that the PM6:Y6 system behaves similarly to the D18-Cl:Y6 system, with $PC_{71}BM$ extending the ink shelf life. Corresponding photovoltaic performance is summarized in **Table S4**. The PM6:Y6 binary devices fabricated from fresh ink exhibit a PCE of 14.24% with an FF of 74.4%, and the binary devices fabricated from aged ink show a rapidly decreasing trend of PCE with the FF drops all the way down to only 51.4% when aged for 20 days. The PM6:Y6:$PC_{71}BM$ ternary devices fabricated from fresh ink exhibit a PCE of 13.39% with an FF of 67.5%. Although the polymer batch utilized was not the best and devices were not extensively optimized, the trends are clear: Even though the performance of ternary devices fabricated from aged ink also decreases with the FF drops to 60.5%, the decrease is much smaller compared to the binaries. The different trends are easy to notice when comparing the *J*–*V* curves of the binary and ternary devices as shown in **Fig. S15**. To extend our method to polymer donors that are not benzodithiophene-based, we added the device data of two PTQ-10 systems and compared the influence of PCBM on the ink shelf life. It is found that the $PC_{71}BM$ can also slow down the ink aging of PTQ-10:Y6 system (see **Table S5**), similar to PM6:Y6. We have also performed experiments for the PM6:N2200 all-polymer system with o-xylene as solvent, given that N2200 (also known as P(NDI_2OD-T_2)) was reported to show strong pre-aggregation.[38] A summary of device performance of PM6:N2200 and PM6:N2200:$PC_{71}BM$ processed with o-xylene is shown in **Table S6**. The addition of PCBM (20% weight ratio) is found to stabilize the PM6:N2200 all-polymer non-chlorinated solvent ink. The ability of PCBM to increase shelf life of the ink is consistent with our model that highly miscible additives prevent excessive aggregation.

Conclusions

In summary, aging of inks for polymer solar cells is a general issue that might prevent commercialization of OSCs. The aging of D18-Cl:Y6 and PM6:Y6 inks were studied, and an approach to decelerate the ink degradation under storage with a highly miscible third component ($PC_{61}BM$ or $PC_{71}BM$) is found effective and delineated. PCBMs are found to reduce the loss in PCE and especially the FF of the devices fabricated from aged inks. The control experiment with perylene red shows that it is indeed the high miscibility of PCBMs with the D18-Cl and Y6 that is the likely causative thermodynamic parameter, which provides a co-solvent effect that suppresses the polymer and NFA pre-aggregation in the inks during storage and hence prevents the formation of large, detrimental domains in the thin films when devices are cast from aged inks. Also, the PCBM can maintain percolation in the mixed-polymer domains that benefits the electron transport. This approach of introducing a hyper-miscible third component to decelerate the ink aging is of great importance to lower the expense of larger area ink-printed organic solar cells and would be a step to their commercialization.

Conflicts of interest

There are no conflicts to declare.

Acknowledgements

The authors gratefully acknowledge the support from the US Office of Naval Research (ONR, grant no. N000142012155) and a UNC General Administration Research Opportunity Initiative grant. X-ray data were acquired at beamlines 7.3.3 and 11.0.1.2 at the ALS, which was supported by the Director, Office of Science, Office of Basic Energy Sciences, of the US Department of Energy under contract no. DE-AC02-05CH11231. The authors thank Dr. Eric Schaible and Dr. Cheng Wang at the ALS for helping with acquisition of X-ray data. The authors also gratefully thank Ms. Mengjin Xu, Dr. Jin Fang and Prof. Chang-Qi Ma at SINANO, CAS for helping with the devices fabrication of PM6:N2200:$PC_{71}BM$ and (D18-Cl:$PC_{61}BM$):Y6 systems.

References

1. Q. Liu, Y. Jiang, K. Jin, J. Qin, J. Xu, W. Li, J. Xiong, J. Liu, Z. Xiao, K. Sun, S. Yang, X. Zhang and L. Ding, *Sci. Bull.*, 2020, **65**, 272-275.
2. Y. Cai, Y. Li, R. Wang, H. Wu, Z. Chen, J. Zhang, Z. Ma, X. Hao, Y. Zhao, C. Zhang, F. Huang and Y. Sun, *Adv. Mater.*, 2021, **33**, 2101733.
3. L. Zhu, M. Zhang, J. Xu, C. Li, J. Yan, G. Zhou, W. Zhong, T. Hao, J. Song, X. Xue, Z. Zhou, R. Zeng, H. Zhu, C. C. Chen, R. C. I. MacKenzie, Y. Zou, J. Nelson, Y. Zhang, Y. Sun and F. Liu, *Nat. Mater.*, 2022, **21**, 656-663.
4. J. Fu, P. W. K. Fong, H. Liu, C.-S. Huang, X. Lu, S. Lu, M. Abdelsamie, T. Kodalle, C. M. Sutter-Fella, Y. Yang and G. Li, *Nat. Commun.*, 2023, **14**, 1760.
5. D. Li, N. Deng, Y. Fu, C. Guo, B. Zhou, L. Wang, J. Zhou, D. Liu, W. Li, K. Wang, Y. Sun and T. Wang, *Adv. Mater.*, 2023, **35**, 2208211.
6. J. Wang, P. Bi, Y. Wang, Z. Zheng, Z. Chen, J. Qiao, W. Wang, J. Li, C. An, S. Zhang, X. Hao and J. Hou, *CCS Chemistry*, 2023, **0**, 1-12.
7. G. Wang, J. Zhang, C. Yang, Y. Wang, Y. Xing, M. A. Adil, Y. Yang, L. Tian, M. Su, W. Shang, K. Lu, Z. Shuai and Z. Wei, *Adv. Mater.*, 2020, **32**, 2005153.
8. Z. Chen, W. Song, K. Yu, J. Ge, J. Zhang, L. Xie, R. Peng and Z. Ge, *Joule*, 2021, **5**, 2395-2407.
9. F. Qin, L. Sun, H. Chen, Y. Liu, X. Lu, W. Wang, T. Liu, X. Dong, P. Jiang, Y. Jiang, L. Wang and Y. Zhou, *Adv. Mater.*, 2021, **33**, 2103017.
10. Y. Han, Z. Hu, W. Zha, X. Chen, L. Yin, J. Guo, Z. Li, Q. Luo, W. Su and C.-Q. Ma, *Adv. Mater.*, 2022, **34**, 2110276.
11. Y.-F. Shen, H. Zhang, J. Zhang, C. Tian, Y. Shi, D. Qiu, Z. Zhang, K. Lu and Z. Wei, *Adv. Mater.*, 2022, DOI: 10.1002/adma.202209030, 2209030.
12. F. Zhao, H. Zhang, R. Zhang, J. Yuan, D. He, Y. Zou and F. Gao, *Adv. Energy Mater.*, 2020, **10**, 2002746.
13. M. Moser, A. Wadsworth, N. Gasparini and I. McCulloch, *Adv. Energy Mater.*, 2021, **11**, 2100056.
14. Y. Li, X. Huang, A. R. Mencke, S. K. Kandappa, T. Wang, K. Ding, Z.-Q. Jiang, A. Amassian, L.-S. Liao, M. E. Thompson and S. R. Forrest, *Proceedings of the National Academy of Sciences*, 2023, **120**, e2301118120.
15. G. Zuo, M. Linares, T. Upreti and M. Kemerink, *Nat. Mater.*, 2019, **18**, 588-593.

16. Y. Jiang, L. Sun, F. Jiang, C. Xie, L. Hu, X. Dong, F. Qin, T. Liu, L. Hu, X. Jiang and Y. Zhou, *Mater. Horiz.*, 2019, **6**, 1438-1443.
17. B. Liu, Y. Han, Z. Li, H. Gu, L. Yan, Y. Lin, Q. Luo, S. Yang and C.-Q. Ma, *Solar RRL*, 2020, **5**, 2000638.
18. G. Zhang, S. A. Hawks, C. Ngo, L. T. Schelhas, D. T. Scholes, H. Kang, J. C. Aguirre, S. H. Tolbert and B. J. Schwartz, *ACS Appl. Mater. Interfaces*, 2015, **7**, 25247-25258.
19. Z. Zheng, E. He, Y. Lu, Y. Yin, X. Pang, F. Guo, S. Gao, L. Zhao and Y. Zhang, *ACS Appl Mater Interfaces*, 2021, **13**, 15448-15458.
20. N. Li, J. D. Perea, T. Kassar, M. Richter, T. Heumueller, G. J. Matt, Y. Hou, N. S. Güldal, H. Chen, S. Chen, S. Langner, M. Berlinghof, T. Unruh and C. J. Brabec, *Nat. Commun.*, 2017, **8**, 14541.
21. X. Du, T. Heumueller, W. Gruber, O. Almora, A. Classen, J. Qu, F. He, T. Unruh, N. Li and C. J. Brabec, *Adv. Mater.*, 2020, **32**, 1908305.
22. M. Ghasemi, H. Hu, Z. Peng, J. J. Rech, I. Angunawela, J. H. Carpenter, S. J. Stuard, A. Wadsworth, I. McCulloch, W. You and H. Ade, *Joule*, 2019, **3**, 1328-1348.
23. M. Ghasemi, N. Balar, Z. Peng, H. Hu, Y. Qin, T. Kim, J. J. Rech, M. Bidwell, W. Mask, I. McCulloch, W. You, A. Amassian, C. Risko, B. T. O'Connor and H. Ade, *Nat. Mater.*, 2021, **20**, 525-532.
24. Y. Zhu, A. Gadisa, Z. Peng, M. Ghasemi, L. Ye, Z. Xu, S. Zhao and H. Ade, *Adv. Energy Mater.*, 2019, **9**, 1900376.
25. Y. Qin, N. Balar, Z. Peng, A. Gadisa, I. Angunawela, A. Bagui, S. Kashani, J. Hou and H. Ade, *Joule*, 2021, **5**, 2129-2147.
26. Z. Wang, Z. Peng, Z. Xiao, D. Seyitliyev, K. Gundogdu, L. Ding and H. Ade, *Adv. Mater.*, 2020, **32**, 2005386.
27. T. Wang and J.-L. Brédas, *J. Am. Chem. Soc.*, 2021, **143**, 1822-1835.
28. A. Zeng, X. Ma, M. Pan, Y. Chen, R. Ma, H. Zhao, J. Zhang, H. Kim, A. Shang, S. Luo, I. C. Angunawela, Y. Chang, Z. Y. Qi, H. Sun, J. Y. L. Lai, H. Ade, W. Ma, F. Zhang and H. Yan, *Adv. Funct. Mater.*, 2021, **31**, 2102413.
29. D.-M. Smilgies, *J. Appl. Crystallogr.*, 2009, **42**, 1030-1034.
30. J. H. Carpenter, A. Hunt and H. Ade, *J. Electron. Spectrosc. Relat. Phenom.*, 2015, **200**, 2-14.
31. B. A. Collins, Z. Li, J. R. Tumbleston, E. Gann, C. R. McNeill and H. Ade, *Adv. Energy Mater.*, 2013, **3**, 65-74.
32. L. Ye, H. Hu, M. Ghasemi, T. Wang, B. A. Collins, J. H. Kim, K. Jiang, J. H. Carpenter, H. Li, Z. Li, T. McAfee, J. Zhao, X. Chen, J. L. Y. Lai, T. Ma, J. L. Bredas, H. Yan and H. Ade, *Nat. Mater.*, 2018, **17**, 253-260.
33. D. R. Kozub, K. Vakhshouri, L. M. Orme, C. Wang, A. Hexemer and E. D. Gomez, *Macromolecules*, 2011, **44**, 5722-5726.
34. L. Ye, S. Li, X. Liu, S. Zhang, M. Ghasemi, Y. Xiong, J. Hou and H. Ade, *Joule*, 2019, **3**, 443-458.
35. H. W. Ro, B. Akgun, B. T. O'Connor, M. Hammond, R. J. Kline, C. R. Snyder, S. K. Satija, A. L. Ayzner, M. F. Toney, C. L. Soles and D. M. DeLongchamp, *Macromolecules*, 2012, **45**, 6587-6599.
36. Z. Peng, X. Jiao, L. Ye, S. Li, J. Rech, W. You, J. Hou and H. Ade, *Chem. Mater.*, 2018, **30**, 3943-3951.
37. J. Yuan, Y. Zhang, L. Zhou, G. Zhang, H.-L. Yip, T.-K. Lau, X. Lu, C. Zhu, H. Peng, P. A. Johnson, M. Leclerc, Y. Cao, J. Ulanski, Y. Li and Y. Zou, *Joule*, 2019, **3**, 1140-1151.
38. R. Steyrleuthner, M. Schubert, I. Howard, B. Klaumünzer, K. Schilling, Z. Chen, P. Saalfrank, F. Laquai, A. Facchetti and D. Neher, *J. Am. Chem. Soc.*, 2012, **134**, 18303-18317.